Light-induced topological superconductivity in transition metal dichalcogenide monolayers

Aleksi Julku [1], Jami J. Kinnunen,[2] Arturo Camacho-Guardian [3] and Georg M. Bruun[1,4]

[1]*Center for Complex Quantum Systems, Department of Physics and Astronomy, Aarhus University, Ny Munkegade,*
DK-8000 Aarhus C, Denmark

[2]*Department of Applied Physics, Aalto University, P.O.Box 15100, 00076 Aalto, Finland*

[3]*Departamento de Física Química, Instituto de Física, Universidad Nacional Autónoma de México,*
Apartado Postal 20-364, Ciudad de México C.P. 01000, Mexico

[4]*Shenzhen Institute for Quantum Science and Engineering and Department of Physics, Southern University of Science*
and Technology, Shenzhen 518055, China

Monolayer transition metal dichalcogenides (TMDs) host deeply bound excitons interacting with itinerant electrons, and as such they represent an exciting new quantum many-body Bose-Fermi mixture. Here, we demonstrate that electrons interacting with a Bose-Einstein condensate (BEC) of exciton-polaritons can realize a two-dimensional topological $p_x + i p_y$ superconductor. Using strong coupling Eliashberg theory, we show that this is caused by an attractive interaction mediated by the BEC, which overcompensates the repulsive Coulomb interaction between the electrons. The hybrid light-matter nature of the BEC is crucial for achieving this, since it can be used to reduce retardation effects and increase the mediated interaction in regimes important for pairing. We finally show how the great flexibility of TMDs allows one to tune the critical temperature of the topological superconducting phase to be within experimental reach.

I. INTRODUCTION

Atomically thin transition metal dichalcogenides (TMDs) are an exciting new class of truly two-dimensional (2D) semiconductors with strong spin-orbit coupling and spin-valley locking, which provides a rich setting for exploring new quantum states and optoelectronic applications [1–3]. Monolayer TMDs exhibit a direct band gap and optical valley selection rules [4–8], and owing to the reduced Coulomb screening they support tightly bound excitons. Furthermore, TMDs in optical microcavities host exciton-polaritons [3,9,10] that allows to combine the nonlinear physics of the matter part with the coherence of photons [3,9,11–17].

Excitons mixed with electrons in TMDs form a new and interesting Bose-Fermi mixtures in a solid-state setting, which compliments such mixtures realised in quantum degenerate atomic gases [18–24]. Bose-Fermi mixtures play a key role in a diverse range of condensed matter phenomena including liquid helium, superconductivity mediated by phonons or magnons, as well as polaron physics. Experiments have so far focused on the regime of small exciton concentration where their interaction with electrons leads to the formation of Fermi polarons [11–13,16,25,26]. Increasing the exciton concentration beyond the polaron regime has been predicted to give rise to a range of intriguing effects such as trion liquids [27], density ordered, and superconducting phases [28–34].

The role of the spin-valley physics of TMDs have however not been fully explored in this context. Here, we show that the flexibility of the spin-valley degrees of freedom provides a promising platform for realising a topological superconductor. This is formed by spin polarized electrons electrons residing in one valley, which interact attractively via an induced interaction mediated by exciton-polaritons in another valley. By tuning the many free parameters of our setup, we show that the critical temperature can be optimised to be within experimental reach. The quest for topological superconductivity remains highly controversial in spite of years of intense effort [35–38], and finally achieving this with our setup would be a major breakthrough.

II. SYSTEM

We consider a TMD monolayer in a microcavity where excitons are created in the K valley by optical pumping. As the Coulomb screening is greatly reduced in 2D, the binding energy [1,39] of excitons is so large that they can for the present purpose be treated as point-like bosons [1,40]. The excitons interact with K'-valley conduction band electrons, which are spin polarized due to intrinsic spin-orbit coupling, see Fig. 1(a). The Hamiltonian of the system is

$$\hat{H} = \sum_{\mathbf{k}} \begin{bmatrix} \hat{x}_{\mathbf{k}}^\dagger \hat{c}_{\mathbf{k}}^\dagger \end{bmatrix} \begin{bmatrix} \epsilon_{\mathbf{k}}^x & \Omega \\ \Omega & \epsilon_{\mathbf{k}}^c \end{bmatrix} \begin{bmatrix} \hat{x}_{\mathbf{k}} \\ \hat{c}_{\mathbf{k}} \end{bmatrix} + \sum_{\mathbf{k}} \epsilon_{\mathbf{k}}^e \hat{e}_{\mathbf{k}}^\dagger \hat{e}_{\mathbf{k}} + \frac{1}{2} \sum_{\mathbf{k},\mathbf{k}',\mathbf{q}} [g_{ee}(\mathbf{q})$$
$$\times \hat{e}_{\mathbf{k}'-\mathbf{q}}^\dagger \hat{e}_{\mathbf{k}+\mathbf{q}}^\dagger \hat{e}_{\mathbf{k}} \hat{e}_{\mathbf{k}'} + g_{xx}(\mathbf{q}) \hat{x}_{\mathbf{k}'-\mathbf{q}}^\dagger \hat{x}_{\mathbf{k}+\mathbf{q}}^\dagger \hat{x}_{\mathbf{k}} \hat{x}_{\mathbf{k}'}]$$
$$+ \sum_{\mathbf{k},\mathbf{k}',\mathbf{q}} g_{ex}(\mathbf{q}) \hat{x}_{\mathbf{k}'-\mathbf{q}}^\dagger \hat{e}_{\mathbf{k}+\mathbf{q}}^\dagger \hat{e}_{\mathbf{k}} \hat{x}_{\mathbf{k}'}, \tag{1}$$

where $\hat{x}_{\mathbf{k}}$, $\hat{e}_{\mathbf{k}}$, and $\hat{c}_{\mathbf{k}}$ annihilate a K-valley exciton, a K'-valley electron, and a cavity photon of momentum $\mathbf{k} = (k_x, k_y)$ respectively. We assume that the electrons occupy states near the conduction band minimum so that their single particle dispersion $\epsilon_{\mathbf{k}}^e = \mathbf{k}^2/2m_e$ is quadratic, and the same argument applies
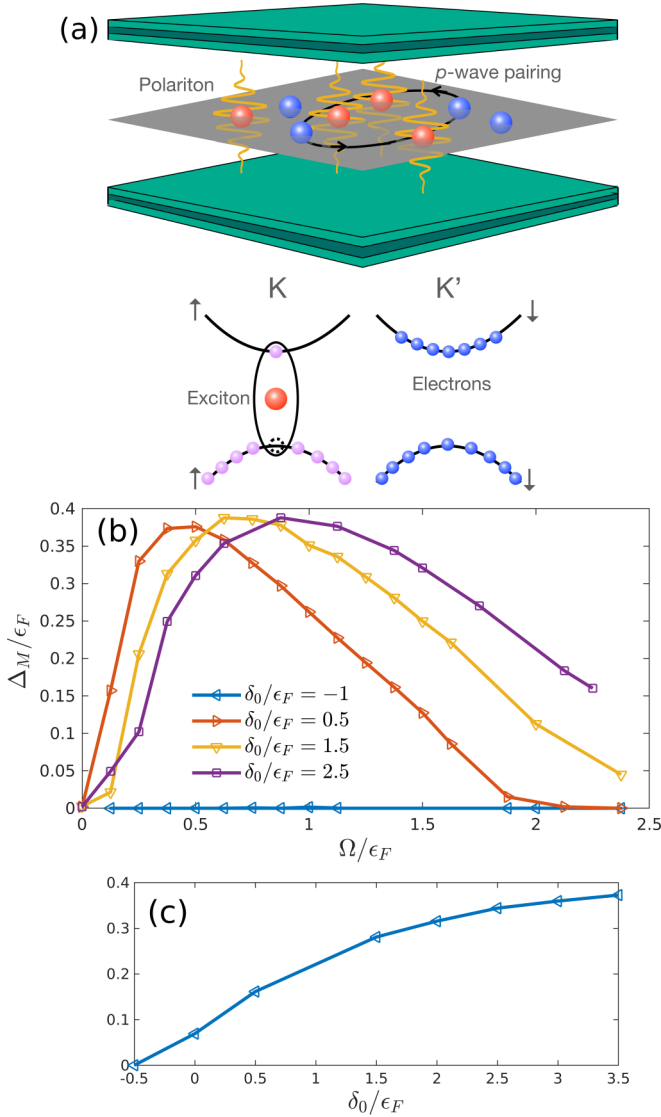
FIG. 1. (a) Upper panel: Spin-polarised electrons (blue spheres) in a monolayer TMD interact with polaritons formed by excitons (red spheres) hybridized with microcavity photons (yellow waves). Polaritons mediate an attractive interaction between the electrons leading to topological *p*-wave pairing (black circle). Lower panel: The excitons are created by particle-hole excitations of spin polarised electrons in the K valley of the TMD band structure, and the electrons live in the K' valley. (b) The superconducting gap Δ_M for different values of δ_0 as a function of Ω. (c) Δ_M as a function of δ_0 for $\Omega/\epsilon_F = 1.375$.

for the excitons giving $\epsilon_{\mathbf{k}}^x = \mathbf{k}^2/2m_x$, with m_e and m_x being the electron and exciton effective masses. The cavity gives rise to a dispersion $\epsilon_{\mathbf{k}}^c = \mathbf{k}^2/2m_c + \delta_0$ for the photons, where δ_0 is the cavity detuning and m_c the photon mass. We use experimentally realistic values of $m_x = 2m_e$, $m_c = 10^{-5}m_e$, and $m_e = 0.5m_0$ with m_0 being the bare electron mass [41]. Furthermore, Ω is the exciton-photon Rabi coupling strength and the second line of Eq. (1) gives the electron-electron and exciton-exciton interaction, whereas the third line is the electron-exciton interaction. We use units where the system volume, Boltzmann's, and Planck's constant are all unity.

Due to the small spatial size of the excitons, the exciton-electron interaction is short range and we therefore assume a momentum independent interaction $g_{ex}(\mathbf{q}) = g_{ex} = 1.5\ \mu\mathrm{eV}\mu\mathrm{m}^2$. This is justified by the fact that we throughout the paper take a small electron density $n_e = k_F^2/4\pi = 10^{15}\ \mathrm{m}^{-2}$ and $n_0/n_e = 10$, if not otherwise mentioned, with k_F being the Fermi momentum and n_0 being the exciton density. The chosen electron density corresponds to a Fermi energy $\epsilon_F = k_F^2/2m_e \lesssim 1$ meV. Since the binding energy of excitons is $\sim$100 meV in TMDs [1], the electrons in valley K' will not significantly change the properties of the excitons in valley K. It has indeed been shown that for large exciton binding energies, they can to a very good approximation be treated as point bosons with a momentum independent (short range) exciton-electron interaction [40], precisely as we do in the present paper. Likewise, we take a momentum independent exciton-exciton interaction. Recent experimental estimates range from $g_{xx} \sim 0.05\ \mu\mathrm{eV}\ \mu\mathrm{m}^2$ [12,42] to $g_{xx} \sim 3.0\ \mu\mathrm{eV}\ \mu\mathrm{m}^2$ [13], and we use $g_{xx} = 0.05\ \mu\mathrm{eV}\ \mu\mathrm{m}^2$ in the following. The Coulomb interaction between the electrons is $g_{ee}(\mathbf{q}) = e^2/2\epsilon q$ where ϵ is the permittivity of the system and e is the electron charge. We use $\epsilon = 4.5\epsilon_0$ with ϵ_0 being the dielectric constant, which is close to the permittivity of boron nitride, a regularly used encapsulating material.

III. MEDIATED INTERACTION

The system is in the regime of strong light-matter coupling leading to the formation of exciton-polaritons with energies $\epsilon_{\mathbf{k}}^{LP/UP} = (\epsilon_{\mathbf{k}}^c + \epsilon_{\mathbf{k}}^x \pm \sqrt{\delta_{\mathbf{k}}^2 + 4\Omega^2})/2$, where $\delta_{\mathbf{k}} = \epsilon_{\mathbf{k}}^c - \epsilon_{\mathbf{k}}^x$ [43]. Recent experiments [14] have revealed signatures of Bose-Einstein condensation of exciton-polaritons in TMDs, and we therefore consider the case where a BEC of density n_0 is formed in the $\mathbf{k} = 0$ state of the lower polariton branch with energy $\epsilon_{\mathbf{k}=0}^{LP}$. Due to its large compressibility, the BEC can mediate a strong and attractive induced interaction whose dominant contribution is the exchange of sound modes in the BEC. Using Bogoliubov theory for the BEC, this yields [44,45]

$$V_{\mathrm{ind}}(\mathbf{k}, i\omega_n) = -\frac{2n_0(g_{ex}\mathcal{C}_0\mathcal{C}_{\mathbf{k}})^2 \tilde{\epsilon}_{\mathbf{k}}^{LP}}{\omega_n^2 + E_{\mathbf{k}}^2}, \qquad (2)$$

for the induced interaction between electrons. Here ω_n is a bosonic Matsubara frequency, $\tilde{\epsilon}_{\mathbf{k}}^{LP} = \epsilon_{\mathbf{k}}^{LP} - \epsilon_0^{LP}$, and $E_{\mathbf{k}} = \sqrt{\tilde{\epsilon}_{\mathbf{k}}^{LP}(\tilde{\epsilon}_{\mathbf{k}}^{LP} + 2g_{xx}\mathcal{C}_0^2\mathcal{C}_{\mathbf{k}}^2 n_0)}$ is the Bogoliubov excitation energy. The Hopfield coefficients $\mathcal{C}_{\mathbf{k}}^2 = 1/2 + \delta_{\mathbf{k}}/2\sqrt{\delta_{\mathbf{k}}^2 + 4\Omega^2}$ in Eq. (2) appear because it is only the excitonic component of the polaritons that interacts with the electrons. In deriving Eq. (2), we have assumed that the BEC density n_0 is much larger than that of the electrons n_e, i.e., $n_0 \gg n_e$, so the BEC is largely unaffected by the electrons. In particular, one can expect there are no roton instabilities in contrast to previous papers focusing on larger electron densities [29,34,46,47], see Appendix A 1.

IV. ELIASHBERG THEORY

Equation (2) shows that the induced interaction is attractive, and we will now explore whether it can overcompensate the repulsive Coulomb interaction between the electrons and

lead to superconductivity. The total electron-electron interaction is

$$V_{\text{tot}}(\mathbf{k}, i\omega_n) = V_{\text{ind}}(\mathbf{k}, i\omega_n) + \frac{e^2}{2\epsilon q[1 + g_{ee}(\mathbf{k})\chi_0(\mathbf{k})]}, \quad (3)$$

where the second term is the screened Coulomb interaction in the random phase approximation, with $\chi_0(\mathbf{k})$ being the static polarizability of the 2DEG [48].

To explore polariton-mediated superconductivity in a reliable way, we use strong coupling Eliashberg theory by defining the matrix Green's function $G_{ij}(\mathbf{k}, \tau)$ [45,48,49],

$$G(\mathbf{k}, \tau) = -\begin{bmatrix} \langle T_\tau \hat{e}_{\mathbf{k}}(\tau)\hat{e}_{\mathbf{k}}^\dagger(0)\rangle & \langle T_\tau \hat{e}_{\mathbf{k}}(\tau)\hat{e}_{-\mathbf{k}}(0)\rangle \\ \langle T_\tau \hat{e}_{-\mathbf{k}}^\dagger(\tau)\hat{e}_{\mathbf{k}}^\dagger(0)\rangle & \langle T_\tau \hat{e}_{-\mathbf{k}}^\dagger(\tau)\hat{e}_{-\mathbf{k}}(0)\rangle \end{bmatrix} \quad (4)$$

where τ is imaginary time and T_τ is the time-ordering operator. Neglecting vertex corrections [48], the normal and anomalous self-energies are [48]

$$G_{11}(p) = \frac{ip_n + \xi_{\mathbf{p}} + \Sigma_{11}(-p)}{\det[G^{-1}(p)]},$$

$$G_{12}(p) = \frac{\Sigma_{12}(p)}{\det[G^{-1}(p)]},$$

$$\Sigma_{ij}(p) = -T \sum_{p'} V_{\text{tot}}(p - p')G_{ij}(p'), \quad (5)$$

where $p \equiv (\mathbf{p}, ip_n)$, p_n is a fermionic Matsubara frequency, T is the temperature, and $\xi_{\mathbf{p}} = \epsilon_{\mathbf{p}} - \mu_e$ with μ_e being the chemical potential for the electrons. Moreover, $G_{22}(p) = -G_{11}(-p)$ and $G_{21}(p) = G_{12}^*(p)$. The symbol $\sum_{p'}$ in Eq. (5) means sum over the Matsubara frequencies and integration over the momenta. We provide a more detailed discussion of these equations in Appendix B.

We solve the Eliashberg equations (5) self-consistently keeping the electron density $n_e = T \sum_p G_{11}(p)e^{ip_n 0^+}$ fixed by adjusting μ_e. A solution with a nonzero value of the gap $\Delta(p) \equiv \Sigma_{12}(p)$ corresponds to the system being in a superconducting phase. Since we consider spin-polarized electrons, the superconducting gap $\Delta(p)$ must be antisymmetric in momentum space. Among the different choices, the $p_x + ip_y$ symmetry is expected to have the lowest energy as it has no nodes. When solving Eq. (5) numerically, we take $\Delta(p) = \Delta_1(|\mathbf{p}|, ip_n)\exp(i\phi_{\mathbf{p}})$, where $\phi_{\mathbf{p}}$ is the polar angle of the momentum $\mathbf{p}$. Thus, our setup naturally realises a topological superconductor with Majorana modes at its edges.

Our approach based on solving the Eliashberg equations should be compared to recent studies of polariton-mediated superconductivity, where the interaction is averaged over the Fermi surface to obtain a BCS-like equation [33], or an analytical approximation based on neglecting the momentum dependence of the self-energies is used [34]. In contrast to these papers, here we take into account the full frequency and momentum dependence of both the superconducting gap $\Delta(p)$ and the diagonal self-energy $\Sigma_{11}(p)$ self-consistently. As shown in Ref. [49], simplified BCS-like theories might dramatically overestimate the critical temperature as compared to the full Eliashberg theory employed here. In particular, it is certainly not guaranteed that our analysis yields a nonzero superconducting order parameter since retardation effects in

general suppress the induced interaction so that the Coulomb repulsion between the electrons may dominate.

V. NUMERICAL RESULTS

We now present results based on solving Eqs. (5) numerically.

A. Pairing close to zero temperature

Let us first focus on the effects of the cavity light as parametrised through the Rabi coupling Ω and detuning δ_0. In Fig. 1(b), the maximum value of the superconducting gap at the Fermi surface, $\Delta_M \equiv \max_\omega \Delta(k_F, \omega)$, is plotted as a function of Ω for different values of the detuning δ_0 and a very low temperature $T = \epsilon_F/50$. We first note that for the negative detuning $\delta_0/\epsilon_F = -1$, Δ_M vanishes and there is no superconductivity. Physically, this is a consequence of the small exciton component of the polariton condensate for $\delta_0 < 0$ as quantified through the Hopfield coefficient $\mathcal{C}_0$. Since the mediated interaction is second order in the electron-exciton interaction, this gives rise to the $\mathcal{C}_0^2$ factor in Eq. (2), which suppresses V_{ind} for negative values of δ_0. Figure 1(c) illustrates this further by plotting Δ_M as a function of δ_0 for $\Omega/\epsilon_F = 1.375$. This shows that the gap is strongly suppressed for $\delta_0 < 0$.

Importantly, we see from Fig. 1(b) that when the light coupling is turned on, the system becomes superconducting. Indeed, while $\Delta_M \simeq 0.002\epsilon_F$ for $\Omega = 0$, which is so small that the corresponding critical temperature is well below the experimentally accessible regime, Δ_M initially increases as a function of Ω, reaching a maximum value at some δ_0-dependent value $\Omega_c > 0$, after which it decreases. To explore why the coupling to light significantly enhances the pairing instability, we define the energy difference $E_{\text{gap}} \equiv \epsilon_0^x - \epsilon_0^{LP} = -\delta_0/2 + \sqrt{\delta_0^2/4 + \Omega^2}$ between the lowest polariton and the bare exciton at zero momentum and plot in Fig. 2(a) Δ_M as a function of E_{gap} by varying Ω for different fixed values of $\delta_0 > 0$. This shows that different δ_0 and Ω that give the same E_{gap} also give approximately the same Δ_M. Hence, the coupling to light mainly affects the pairing through E_{gap} when $\delta_0 > 0$. To understand this, we plot in Fig. 2(b) the single particle dispersion $\epsilon_{\mathbf{k}}^{LP}$ for $\delta_0/\epsilon_F = 1/2$ and $\Omega/\epsilon_F = \sqrt{3/2}$. Due to the small photon mass m_c, the polariton dispersion is very steep around the origin and the photons decouple for momenta $k \ll k_F$ such that the dispersion of the lower polariton approaches that of the bare exciton with the corresponding Hopfield coefficient close to unity. Hence, the main effect of the light coupling is indeed to introduce the energy gap E_{gap} between the ground state polaritons forming the BEC and its excitations mediating the attractive interaction between the electrons.

To further explore the role of E_{gap}, it is instructive for a moment to approximate the polariton dispersion as $\epsilon_{\mathbf{k}}^{LP} \approx \epsilon_{\mathbf{k}}^x - E_{\text{gap}}\delta_{\mathbf{k},0}$ with $\delta_{\mathbf{k},0}$ being the Kronecker delta. We have checked numerically that this gives essentially the same results as using the full exciton-polariton spectrum. Figure 3(a) plots the induced interaction V_{ind}, given in Eq. (2), as a function of $\tilde{\epsilon}^{LP}$ and ω_n by taking $\mathcal{C}_{\mathbf{k}}\mathcal{C}_0 \approx 1$, which is a reasonable approximation for $\delta_0 > 0$. The relevant momenta for superconductivity are $k \lesssim \mathcal{O}(k_F)$ corresponding to polariton energies $E_{\text{gap}} \lesssim \tilde{\epsilon}_{\mathbf{k}}^{LP} \lesssim E_{\text{gap}} + \epsilon_F$, and the important frequencies are likewise
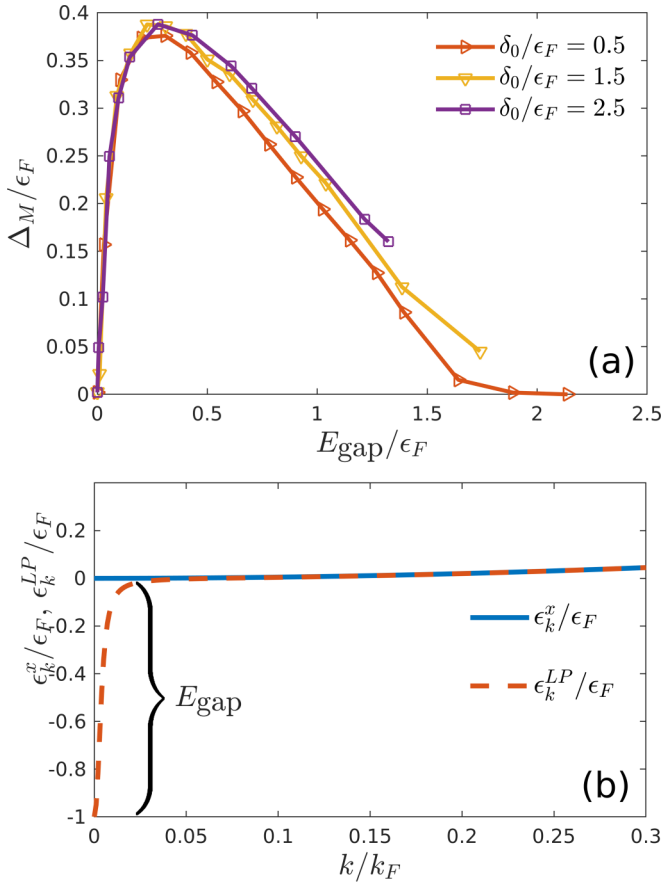
FIG. 2. (a) Δ_M for different δ_0 as a function of E_{gap}. (b) Exciton dispersion $\epsilon_{\mathbf{k}}^x$ (solid blue) and a typical exciton-polariton dispersion $\epsilon_{\mathbf{k}}^{LP}$ (red dashed). The energy difference $\epsilon_0^x - \epsilon_0^{LP}$ is denoted as E_{gap}.

FIG. 3. (a) The induced interaction V_{ind} as a function of $\tilde{\epsilon}^{LP}$ and ω for $\mathcal{C}_0 \mathcal{C}_{\mathbf{k}} \approx 1$. White and red rectangles represent the relevant regime for pairing for $E_{\text{gap}}/\epsilon_F = 0$ and $E_{\text{gap}}/\epsilon_F = 0.5$, respectively. (b) V_{ind} as a function of ω_n for different momenta in the case of excitons (dashed) and exciton-polaritons (solid) with $\delta_0/\epsilon_F = \Omega/\epsilon_F = 0.5$ ($E_{\text{gap}}/\epsilon_F = 0.31$). (c) Momentum distribution $n_{\mathbf{k}}$ for $\delta_0/\epsilon_F = 1$ and $\Omega/\epsilon_F = 0.125$ ($E_{\text{gap}}/\epsilon_F = 0.015$, blue), $\Omega/\epsilon_F = 0.875$ ($E_{\text{gap}}/\epsilon_F = 0.5$, red), and $\Omega/\epsilon_F = 1.625$ ($E_{\text{gap}}/\epsilon_F = 1.2$, yellow).

$|\omega| \lesssim \epsilon_F$. The corresponding region is indicated as rectangles in Fig. 3(a) for $E_{\text{gap}}/\epsilon_F = 0$ and $E_{\text{gap}}/\epsilon_F = 0.5$. We see that the magnitude of V_{ind} decreases for large $\tilde{\epsilon}_{\mathbf{k}}^{LP}$, which is easily understood by the fact that $V_{\text{ind}} \propto 1/\tilde{\epsilon}_{\mathbf{k}}^{LP}$. This explains the suppression of superconductivity for large E_{gap} shown in Fig. 2(a). The initial increase in the pairing with E_{gap} is, on the other hand, caused by two effects.

First, it follows from Eq. (2) that V_{ind} becomes less dependent on ω with increasing E_{gap}. Namely, the full width at half maximum of V_{ind} in the frequency space at finite $\mathbf{k}$ is given by the Bogoliubov energy, i.e. $E_{\mathbf{k}} = \sqrt{(\epsilon_{\mathbf{k}}^x + E_{\text{gap}})^2 + 2n_0 g_{xx}(\epsilon_{\mathbf{k}}^x + E_{\text{gap}})}$ for $\mathcal{C}_{\mathbf{k}} \mathcal{C}_0 \approx 1$. Polaritons with a nonzero E_{gap} thus yield a broader interaction in frequency space suppressing retardation, which in turn enhances Cooper pairing [48,49]. Second, V_{ind} increases for energies $\tilde{\epsilon}_{\mathbf{k}}^{LP} \lesssim \omega$. Figure 3(a) shows that these two effects make the induced interaction less dependent on frequency as well as larger in the region relevant for pairing when $E_{\text{gap}} \sim \epsilon_F/2$. This explains the maximum in the pairing amplitude shown in Fig. 2(a).

One should note that we ignored the dependence of $\mathcal{C}_0$ on δ_0 and Ω by setting it to unity in the discussion above. This approximation is based on the fact when $\delta_0 \gg \Omega$ ($E_{\text{gap}} \ll \Omega$), polaritons are predominantly excitonic and $\mathcal{C}_0 \sim 1$. This is reflected in Fig. 2(a) where Δ_M essentially depends only on
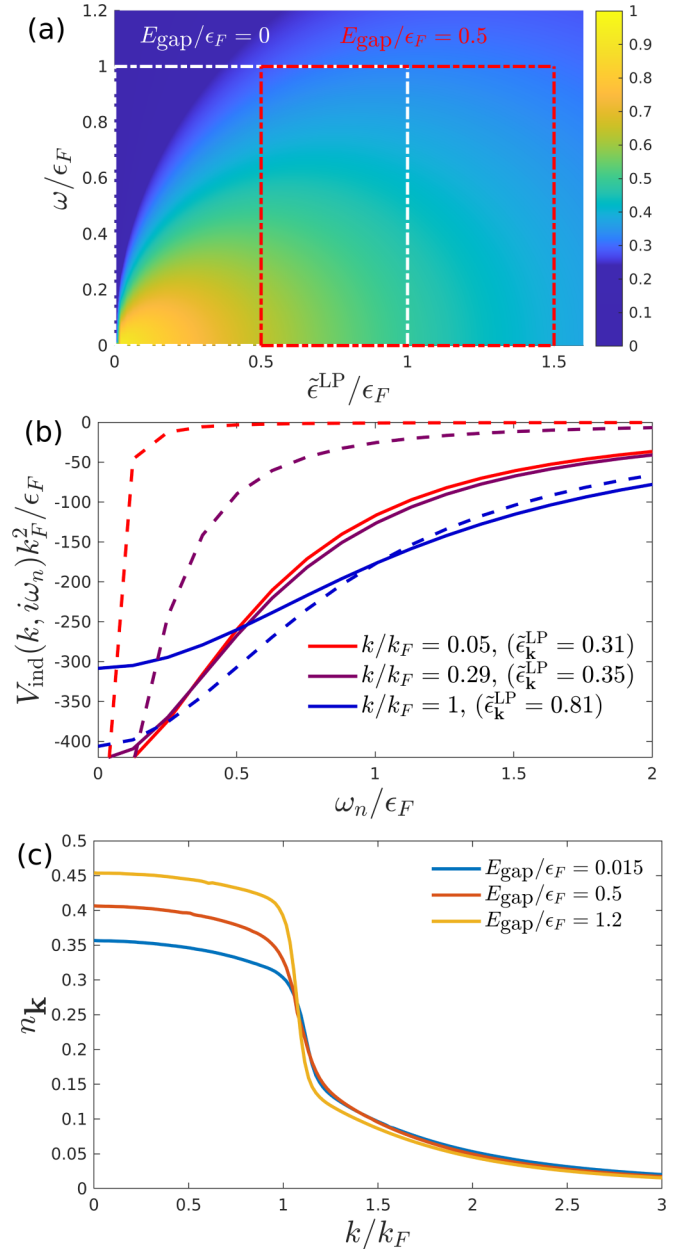
E_{gap} for $E_{\text{gap}} \ll \Omega$. For larger values of E_{gap}, the results for different δ_0 start to deviate from each other because the approximation $\mathcal{C}_0 \sim 1$ breaks down. In this limit, V_{ind} depends on $\mathcal{C}_0$, which is a function of δ_0 and Ω in a way that cannot be expressed in terms of the single parameter E_{gap}, see also Appendix A 2. Likewise, when $\delta_0 < 0$, the dependence of the gap on the different parameters cannot be expressed through the single parameter E_{gap} due to fact that $\mathcal{C}_0 < 1/2$ depends on Ω and δ_0.
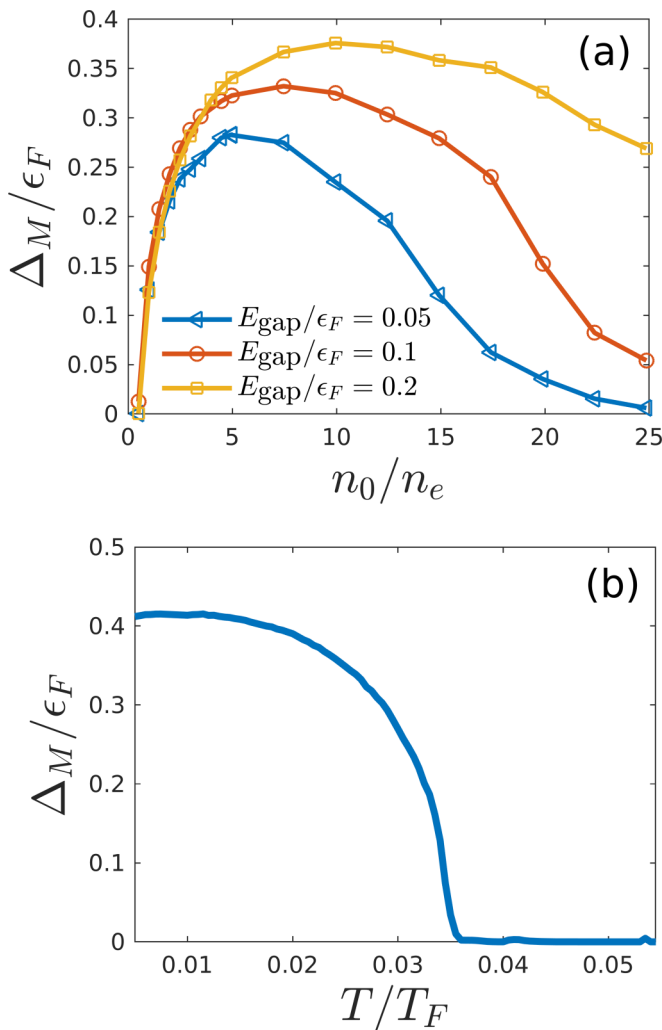
FIG. 4. (a) Δ_M as a function of n_0 for $\delta_0/\epsilon_F = 1$, $\Omega_0/\epsilon_F = 0.23$ ($E_{gap}/\epsilon_F = 0.05$, blue), $\delta_0/\epsilon_F = 1$, $\Omega_0/\epsilon_F = 0.33$ ($E_{gap}/\epsilon_F = 0.1$, red), and $\delta_0/\epsilon_F = 1$, $\Omega_0/\epsilon_F = 0.49$ ($E_{gap}/\epsilon_F = 0.2$, yellow). (b) Δ_M as a function of temperature for $\delta_0/\epsilon_F = 5$ and $\Omega/\epsilon_F = 1.37$ ($E_{gap}/\epsilon_F = 0.35$).

To further demonstrate the reduced retardation effects caused by the light coupling, in Fig. 3(b) we plot V_{ind} as a function of ω for different momenta **k** both in case of excitons (dashed lines) and exciton-polaritons (solid lines) for $\delta_0/\epsilon_F = \Omega/\epsilon_F = 0.5$ ($E_{gap}/\epsilon_F = 0.31$). Here the full dependence of V_{ind} on the Hopfield coefficients is taken into account. We see that introducing the coupling to light makes V_{ind} broader in the frequency space as well as a larger for momenta **k** corresponding to $\tilde{\epsilon}_{\mathbf{k}}^{LP} \lesssim \omega$, in agreement with the discussion above. The suppression of retardation effects due to polaritons is also illustrated in Fig. 3(c), where the momentum distribution function $n_{\mathbf{k}} = \langle \hat{e}_{\mathbf{k}}^{\dagger} \hat{e}_{\mathbf{k}} \rangle$ of the electrons is plotted for different values of E_{gap}. Increasing E_{gap} sharpens the Fermi surface as the frequency dependence of the diagonal self-energy Σ_{11} decreases as shown in Appendix C, thereby enhancing superconductivity [48].

So far we have kept the density ratio constant at $n_0/n_e = 10$. In Fig. 4(a), we plot the gap Δ_M as a function of the BEC density n_0. This shows that it depends nonmonotonically on

n_0, vanishing both for small and large n_0, reaching a maximum value in between. It should be noted that the polaritons likely are affected by the electrons when $n_0 \lesssim n_e$, which is not taken into account by our theory. The result of Fig. 4(a) showing that superconductivity is lost for $n_0 \rightarrow 0$ is however physically robust, since it is caused by the interaction mediated by the condensate being proportional to its density, i.e., $V_{ind} \propto n_0$ in Eq. (2). The suppression of superconductivity shown in Fig. 4 for large n_0 can on the other hand be explained by the fact that the range of the induced interaction is determined by the BEC coherence length, i.e., $\xi \sim 1/\sqrt{2m_x(E_{gap} + 2n_0 g_{xx})}$, see Appendix A 3. Increasing n_0 thus reduces the induced interaction range leading to suppression of the Cooper pairing. Similar results regarding the density dependence of pairing were reported for atomic Bose-Fermi mixtures [45,49].

B. Temperature dependence

The critical temperature of the topological superconducting phase is obviously an experimentally important quantity. To investigate this, we plot in Fig. 4(b) the gap Δ_M as a function of temperature for $\delta_0/\epsilon_F = 5$ and $\Omega/\epsilon_F = 1.37$ ($E_{gap}/\epsilon_F = 0.35$). These parameters are chosen so that Δ_M is close to its maximum value, see Fig. 2(b). This demonstrates that the critical temperature is $T_c \simeq 0.035 T_F$, which corresponds to $T_c \sim 0.4$ K for $n_e = 10^{15}$ m^{-2}. Importantly, such low temperatures are within experimental reach using, e.g., a He-3/He-4 dilution refrigerator [50] that gives access to temperatures down to tens of mK. Note that the ratio $T_c/\Delta_M(T = 0) \sim 0.085$ is an order of magnitude smaller than the usual BCS result 0.57. This is due to the momentum and frequency dependence of V_{ind}, causing the superconducting gap to be peaked at the Fermi surface as shown in Appendix C, and thus the Cooper pairs more loosely bound than in case of the constant BCS gap. Other strong coupling effects such as the blurring of the Fermi surface also contribute to this effect [48]. Moreover, in contrast to the BCS result, the value of $T_c/\Delta_M(T = 0)$ is not universal but depends on the values of the physical parameters.

VI. DISCUSSION AND OUTLOOK

We demonstrated that electrons interacting with an exciton-polariton BEC in a monolayer TMD represent a promising system to observe a 2D topological superconductor. The coupling to light was shown to be crucial for achieving this, since it suppresses the retardation effects and makes the induced interaction stronger in regions important for pairing. We note that this conclusion is reliable, since it is based on a well-known expression for the induced interaction mediated by sound modes of a BEC, generalised to the hybrid light-matter case at hand. An appealing feature of our proposal is its large degree of flexibility. Experimentally, one can tune the Rabi splitting, the cavity detuning, and the densities of the BEC and electrons to optimize the range and relative strength of the pairing interaction and thereby increase the critical temperature.

In contrast to earlier works exploring polariton-mediated superconductivity with trivial topology in multilayer setups [33,34], the spin-valley degrees of freedom of our single layer

TMD system naturally realises a topological superconductor. In addition, using the flexibility of our system, we achieve a critical temperature comparable to that of Ref. [34] despite the fact that our electron density is roughly one hundred times smaller.

While we have used equilibrium theory to describe the condensate, it is intrinsically in a nonequilibrium steady-state determined by the balance between a pump laser and the continuous photon loss through the cavity mirrors. This steady-state can be described using a generalised Bogoliubov theory that yields an excitation spectrum of the same form as the one used here, where the chemical potential is replaced by the frequency of the pump laser [51]. The dissipation of the polaritons due to photon leaking out of the cavity is more-over strongly suppressed for the phonon modes mediating the attractive interaction between the electrons, since polaritons are almost purely excitonic. Indeed, their damping rate is given by $\gamma_{\mathbf{k}}^{LP} = \mathcal{S}_{\mathbf{k}}^2 \gamma_c$, with γ_c being the photon damping rate and $\mathcal{S}_{\mathbf{k}}^2 = 1 - \mathcal{C}_{\mathbf{k}}^2 \ll 1$ their photonic component, which is strongly suppressed expect for very small momenta. Furthermore, since $E_{\text{gap}} \sim \Omega \gg \gamma_c$ for the maximal pairing gap, the effects of photon losses on the Bogoliubov spectrum are further suppressed. For these reasons, we expect our results to be reliable for the pump-loss setup considered even though we have applied equilibrium theory.

The external pump can also cause heating effects on the sample, especially if one wants to achieve high polariton densities. However, the heating effects on the electrons can be avoided by using a bilayer setup [52,53] where excitons and electrons exist in separate layers and their interaction is tuned via the Feshbach resonance. In this case the heating effects of the pump does not affect electrons, and at the same time the electron-exciton interaction can be tuned. This can furthermore be used to increase the critical temperature, which is an interesting topic for future investigations.

Our results open up several other new research directions into polariton-mediated superconductivity. This includes treating the back-action of the electrons onto the excitons as well as the effects of superconductivity on the screening of the Coulomb interaction within the Eliashberg framework. One could also explore bilayer TMDs, where a relative twist angle produces a long-wavelength moiré lattice and flat Bloch bands [54–56]. One has already observed excitons in moiré lattices [57–61], and flat bands give rise to strong correlations and nontrivial superfluid properties [62–65]. Furthermore, polariton-mediated ferromagnetism has been recently observed in moiré TMDs [66]. In general, there are a plethora of interesting questions concerning interacting Bose-Fermi mixtures that can be addressed using exciton-electron mixtures in TMDs, which will most likely complement the substantial experimental effort investigating atomic Bose-Fermi mixtures [18–24].

ACKNOWLEDGMENTS

APPENDIX A: BEC-MEDIATED INTERACTION

Here we show the derivation for the induced electron-electron interaction $V_{\text{ind}}(\mathbf{k}, i\omega_n)$, i.e., Eq. (2) of the main text, arising due to the exchange of sound modes of the Bose-Einstein condensation (BEC) of polaritons. The starting point is the electron-exciton interaction

$$\hat{H}_{\text{e-x}} = g_{ex} \sum_{\mathbf{k},\mathbf{k}',\mathbf{q}} \hat{x}_{\mathbf{k}'-\mathbf{q}}^\dagger \hat{e}_{\mathbf{k}+\mathbf{q}}^\dagger \hat{e}_{\mathbf{k}} \hat{x}_{\mathbf{k}'} \quad (A1)$$

where the system area is taken to be unity, $\hat{e}_{\mathbf{k}}^\dagger$ ($\hat{x}_{\mathbf{k}}^\dagger$) annihilates an electron (exciton) of momentum $\mathbf{k}$ and we have assumed a contact interaction g_{ex}. To take into account the light-matter coupling and the emergence of polaritons, we write the exciton operator as $\hat{x}_{\mathbf{k}} = \mathcal{S}_{\mathbf{k}}\hat{\gamma}_{\mathbf{k}}^{UP} + \mathcal{C}_{\mathbf{k}}\hat{\gamma}_{\mathbf{k}}^{LP}$, where $\mathcal{C}_{\mathbf{k}}^2 = 1/2 + \delta_{\mathbf{k}}/(2\sqrt{\delta_{\mathbf{k}}^2 + 4\Omega^2})$ and $\mathcal{S}_{\mathbf{k}}^2 = 1 - \mathcal{C}_{\mathbf{k}}^2$ are the Hopfield coefficients and $\hat{\gamma}_{\mathbf{k}}^{LP}$ ($\hat{\gamma}_{\mathbf{k}}^{UP}$) is the annihilation operator for the lower (upper) branch exciton-polariton of momentum $\mathbf{k}$ and energy $\epsilon_{\mathbf{k}}^{LP}$ ($\epsilon_{\mathbf{k}}^{UP}$). As the condensation takes place within the lower polariton branch, we can safely discard the upper polariton branch to recast Eq. (A1) as

$$\hat{H}_{\text{e-x}} = g_{ex} \sum_{\mathbf{k},\mathbf{k}',\mathbf{q}} \mathcal{C}_{\mathbf{k}'}\mathcal{C}_{\mathbf{k}'-\mathbf{q}} \hat{\gamma}_{\mathbf{k}'-\mathbf{q}}^\dagger \hat{e}_{\mathbf{k}+\mathbf{q}}^\dagger \hat{e}_{\mathbf{k}} \hat{\gamma}_{\mathbf{k}'} \quad (A2)$$

where for simplicity we have denoted $\hat{\gamma}_{\mathbf{k}} \equiv \hat{\gamma}_{\mathbf{k}}^{LP}$. In the same way, exciton-exciton interaction is now written as

$$\hat{H}_{\text{x-x}} = g_{xx} \sum_{\mathbf{k},\mathbf{k}',\mathbf{q}} \hat{x}_{\mathbf{k}'-\mathbf{q}}^\dagger \hat{x}_{\mathbf{k}+\mathbf{q}}^\dagger \hat{x}_{\mathbf{k}} \hat{x}_{\mathbf{k}'}$$
$$\approx g_{xx} \sum_{\mathbf{k},\mathbf{k}',\mathbf{q}} \mathcal{C}_{\mathbf{k}'-\mathbf{q}}\mathcal{C}_{\mathbf{k}+\mathbf{q}}\mathcal{C}_{\mathbf{k}}\mathcal{C}_{\mathbf{k}'} \hat{\gamma}_{\mathbf{k}'-\mathbf{q}}^\dagger \hat{\gamma}_{\mathbf{k}+\mathbf{q}}^\dagger \hat{\gamma}_{\mathbf{k}} \hat{\gamma}_{\mathbf{k}'}. \quad (A3)$$

As the polaritons condense at $\mathbf{k} = 0$, we can take $\hat{\gamma}_{\mathbf{k}} \approx \sqrt{n_0}\delta_{\mathbf{k},0} + \delta\hat{\gamma}_{\mathbf{k}}$, where n_0 is the condensate density and $\delta\hat{\gamma}_{\mathbf{k}}$ describes the fluctuations around the BEC ground state, with $\langle \delta\hat{\gamma}_{\mathbf{k}} \rangle = 0$. In order to treat the polariton-mediated interaction, it is useful to define the 2x2 bosonic Green's function for polaritons as

$$G_B(\mathbf{k}, \tau)$$
$$\equiv -\left\langle T_\tau \begin{bmatrix} \delta\hat{\gamma}_{\mathbf{k}}(\tau) \\ \delta\hat{\gamma}_{-\mathbf{k}}^\dagger(\tau) \end{bmatrix} [\delta\hat{\gamma}_{\mathbf{k}}^\dagger(0) \quad \delta\hat{\gamma}_{-\mathbf{k}}(0)] \right\rangle$$
$$= \begin{bmatrix} -\langle T_\tau \delta\hat{\gamma}_{\mathbf{k}}(\tau)\delta\hat{\gamma}_{\mathbf{k}}^\dagger(0)\rangle & -\langle T_\tau \delta\hat{\gamma}_{\mathbf{k}}(\tau)\delta\hat{\gamma}_{-\mathbf{k}}(0)\rangle \\ -\langle T_\tau \delta\hat{\gamma}_{-\mathbf{k}}^\dagger(\tau)\delta\hat{\gamma}_{\mathbf{k}}^\dagger(0)\rangle & -\langle T_\tau \delta\hat{\gamma}_{-\mathbf{k}}^\dagger(\tau)\delta\hat{\gamma}_{-\mathbf{k}}(0)\rangle, \end{bmatrix}$$
$$(A4)$$

where T_τ is the time ordering operator and τ is the imaginary time. Now, within the Bogoliubov theory, we expand the polariton-polariton interaction in Eq. (A3) up to the second order in the fluctuation operators and ensure that terms linear in $\hat{\gamma}_{\mathbf{k}=0}$ vanish by the virtue of the Hughenholtz-Pines theorem (such that the BEC is a stable ground state). Consequently, one can cast the inverse of the 2×2 bosonic Green's function for

the polaritons in the Matsubara frequency space as

$$G_B^{-1}(\mathbf{k}, i\omega_n)$$

$$= \begin{bmatrix} i\omega_n - \tilde{\epsilon}_{\mathbf{k}}^{LP} - g_{xx}\mathcal{C}_0^2\mathcal{C}_{\mathbf{k}}^2 n_0 & -g_{xx}\mathcal{C}_0^2\mathcal{C}_{\mathbf{k}}^2 n_0 \\ -g_{xx}\mathcal{C}_0^2\mathcal{C}_{\mathbf{k}}^2 n_0 & -i\omega_n - \tilde{\epsilon}_{\mathbf{k}}^{LP} - g_{xx}\mathcal{C}_0^2\mathcal{C}_{\mathbf{k}}^2 n_0 \end{bmatrix}$$

$$(A5)$$

Here $\mathbf{k} \neq 0$, ω_n is a bosonic Matsubara frequency and $\tilde{\epsilon}_{\mathbf{k}}^{LP} \equiv \epsilon_{\mathbf{k}}^{LP} - \epsilon_0^{LP}$. The Bogoliubov excitation energies $E_{\mathbf{k}} = \sqrt{\tilde{\epsilon}_{\mathbf{k}}^{LP}(\tilde{\epsilon}_{\mathbf{k}}^{LP} + 2g_{xx}\mathcal{C}_0^2\mathcal{C}_{\mathbf{k}}^2 n_0)}$ are obtained as the poles of G_B.

We can now derive the BEC-mediated electron-electron interaction. By using the form $\hat{\gamma}_{\mathbf{k}} \approx \sqrt{n_0}\delta_{\mathbf{k},0} + \delta\hat{\gamma}_{\mathbf{k}}$ in Eq. (A2), keeping the terms up to the linear order in the fluctuation operators $\delta\hat{\gamma}_{\mathbf{k}}$ and ignoring constant shifts in the electronic chemical potential, we obtain

$$\hat{H}_{\text{e-x}} = g_{ex}\sqrt{n_0}\sum_{\mathbf{k},\mathbf{q}} \mathcal{C}_0\mathcal{C}_{\mathbf{k}}\hat{e}_{\mathbf{k}+\mathbf{q}}^{\dagger}\hat{e}_{\mathbf{k}}\left(\delta\hat{\gamma}_{\mathbf{q}} + \delta\hat{\gamma}_{-\mathbf{q}}\right). \qquad (A6)$$

This is of the same form as the electron-phonon coupling responsible for the phonon-mediated superconductivity. By following the usual procedure, i.e., writing down the perturbation expansion for the electronic Green's function [67], it is straightforward to show that the interaction (A6) leads to the effective electron-electron interaction of the form

$$\hat{H}_{\text{ind}} = \frac{1}{2}\sum_{\mathbf{k},\mathbf{k}',\mathbf{q}} \left(\sum_{ij}^{2}[G_B(\mathbf{q}, \tau)]_{ij}g_{ex}^2 n_0(\mathcal{C}_0\mathcal{C}_{\mathbf{k}})^2\right)$$

$$\times \hat{e}_{\mathbf{k}+\mathbf{q}}^{\dagger}\hat{e}_{\mathbf{k}'-\mathbf{q}}^{\dagger}(\tau)\hat{e}_{\mathbf{k}'}(\tau)\hat{e}_{\mathbf{k}}$$

$$\equiv \frac{1}{2}\sum_{\mathbf{k},\mathbf{k}',\mathbf{q}} V_{\text{ind}}(\mathbf{q}, \tau)\hat{e}_{\mathbf{k}+\mathbf{q}}^{\dagger}\hat{e}_{\mathbf{k}'-\mathbf{q}}^{\dagger}(\tau)\hat{e}_{\mathbf{k}'}(\tau)\hat{e}_{\mathbf{k}}, \qquad (A7)$$

where $\mathbf{q} \neq 0$. With the Bogoliubov Green's function Eq. (A5), the induced interaction V_{ind} can be written in the Matsubara space as

$$V_{\text{ind}}(\mathbf{k}, i\omega_n) = g_{ex}^2 n_0(\mathcal{C}_0\mathcal{C}_{\mathbf{k}})^2 \sum_{ij}^{2}[G_B(\mathbf{k}, i\omega_n)]_{ij}$$

$$= -\frac{g_{ex}^2 n_0(\mathcal{C}_0\mathcal{C}_{\mathbf{k}})^2\tilde{\epsilon}_{\mathbf{k}}^{LP}}{\omega_n^2 + E_{\mathbf{k}}^2}, \qquad (A8)$$

which is Eq. (2) in the main text. The Feynman diagrams of $V_{\text{ind}}(\mathbf{k}, i\omega_n)$ are shown in Fig. 5 and Eq. (A8) can be easily obtained from them in a straightforward manner by using the standard rules for the bosonic propagators [68].

1. Possible roton instabilities of the Bogoliubov spectrum

In Refs. [29,34], where a bilayer setup of electrons residing in one layer and exciton-polaritons in a separate TMD monolayer was considered, it was shown that the electron-hole excitations of the electron sea can lead to a supersolid instability of the Bose-condensed polariton gas, i.e., the Bogoliubov energy $E_{\mathbf{k}}$ reaches the zero energy at finite momentum, leading to the breakdown of the assumption on the zero-momentum BEC. In Ref. [34] it was argued that this instability enhances the critical temperature for superconductivity in the parameter regime near the instability. As we consider electron
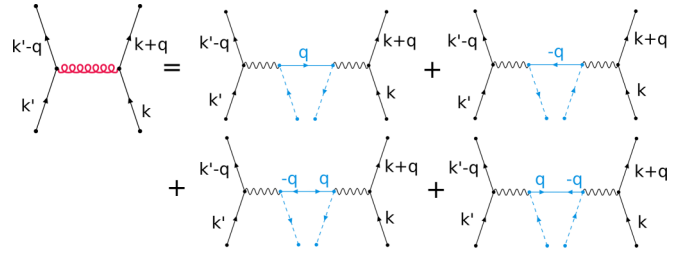

FIG. 5. Feynman diagrams for induced interaction $V_{\text{ind}}(\mathbf{k}, i\omega_n)$. The red-curled line denotes V_{ind}, black-wiggly lines are the bare vertex $g_{ex}\mathcal{C}_0\mathcal{C}_{\mathbf{q}}$, dashed-blue (solid) lines are the polariton propagators of the condensate (Bogoliubov excitations) and black-solid lines are electron propagators.

densities much smaller than the exciton density, we expect that such an instability does not take place in our system. Despite this and the fact that the electron densities we consider ($\sim 10^{15}\text{m}^{-2}$) are much smaller than those investigated in Ref. [33] (4×10^{16} m^{-2}) and in Ref. [34] ($\sim 10^{17}$ m^{-2}), we predict a superconducting critical temperature $T_c \sim 1$ K of our monolayer setup, which is of the same order of magnitude as the maximum predicted in Ref. [34] for the bilayer system before a supersolid instability sets in. Reasons for this difference between our and Refs. [33,34] include the different momentum dependence of the electron-exciton interaction: In our monolayer setup, the excitons are tightly bound and therefore the exciton-electron interaction can be taken to be momentum-independent [40]. This is in stark contrast to the bilayer system considered in Refs. [33,34], where the exciton-electron interaction is strongly momentum-dependent.

It should be noted that the random phase approximation (RPA) analysis used in Ref. [34] to reveal possible supersolid instabilities would not be self-consistent in our case. Namely, the Eliashberg theory is a second order theory with respect to the exciton-electron interaction g_{ex}. On the other hand, the RPA renormalizes the exciton-exciton interaction as $g_{xx} \rightarrow g_{xx} + g_{ex}^2\chi_{RPA}(\mathbf{k})$, where $\chi_{RPA}(\mathbf{k})$ is the RPA polarization bubble of the electron gas [34]. If one was to include the back-action of electrons on polaritons via the RPA, then the resulting induced interaction (A8) would not be anymore in the 2nd order of g_{ex} as the renormalized Bogoliubov energies $E_{\mathbf{k}}$ would already include g_{ex} via the renormalization of the exciton-exciton interaction. Hence, the theory would not be self-consistent and, as a result, *RPA can lead to unphysical roton minima*. To fix this, one would need to use the full Eliashberg Green's functions in the back-action, in contrast to the ideal Fermi gas polarization bubble used in Ref. [34]. One would then proceed to compute the new Bogoliubov modes and new solutions for Eliashberg equations and continue this process iteratively till both the Bogoliubov and Eliashberg solution would converge. Such a self-consistent approach is computationally a very heavy task to implement and is thus out of scope of our paper. It is important to note that the simplistic approach of Ref. [34] implies that the emergence of the roton minimum can actually enhance the superconducting temperature near the instability. A possibility to find roton minima in the setup considered in this work therefore remains an interesting topic for future BEC-mediated superconductivity studies.
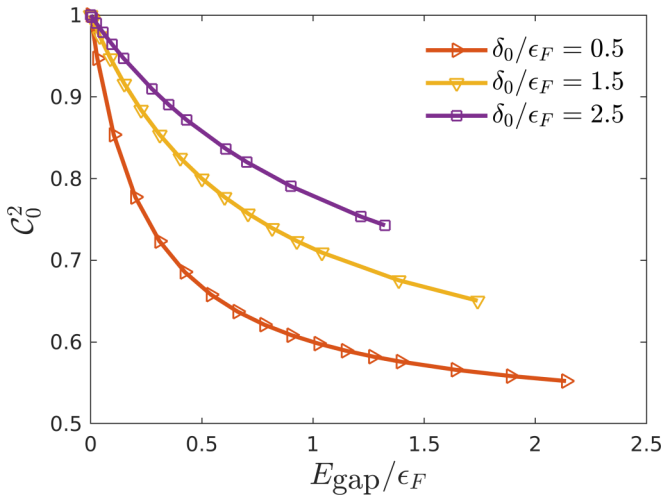
FIG. 6. Hopfield coefficient $\mathcal{C}_0^2$ as a function of E_{gap} for three different values of δ_0.

Roton-like instabilities have been also predicted in TMD monolayer systems in Refs. [46,47]. In Ref. [46] nonzero momentum condensate states of excitons are shown to arise from the population imbalance between the holes and electrons that form excitons. In our case, there is not such a population imbalance between holes and electrons and therefore the results of Ref. [46] do not apply in our case. The roton minima described in Ref. [47], on the other hand, arise for a single exciton immersed in a Fermi sea of electrons via the Pauli blocking. This is the extreme opposite regime of what we consider, where we take the electron density to be much smaller than the exciton density. Moreover, the electrons forming the exciton are the same as those in the Fermi sea, whereas in our study they reside in different valleys. The results of Ref. [47], while interesting, are therefore not of direct relevance to our paper.

2. The role of the Hopfield coefficients

The main features and behavior of the induced interaction V_{ind} can be understood fairly well as a function of E_{gap} by approximating $\mathcal{C}_k^2 \approx 1$ and $\mathcal{C}_0^2 \approx 1$ as is done in Fig. 3(a) of the main text. For finite **k** this is indeed a feasible approximation as the photons decouple from excitons at momenta that are much smaller than the ones relevant for pairing [see Fig. 2(b) in the main text]. However, $\mathcal{C}_0^2$ can in principle deviate from unity and thus affect the induced interaction strength in a nontrivial way.

In Fig. 6 we plot $\mathcal{C}_0^2$ as a function of E_{gap} for three different values of δ_0 that were used in Fig. 2(a) of the main text. We see that for small E_{gap} the Hopfield coefficients are close to unity and become gradually smaller as a function of increasing E_{gap}. The effect is largest for smaller δ_0, consistent with the fact that smaller δ_0 implies larger photonic component and thus smaller $\mathcal{C}_0$. From Fig. 2(a) of the main text we see that the pairing gap Δ_M is maximized around $E_{\text{gap}}/\epsilon_F \sim 0.25$ and all three cases of δ_0 yield roughly the same Δ_M. On the other hand, from Fig. 6 we see that the corresponding $\mathcal{C}_0^2$ values are 0.75 and 0.92 for $\delta_0/\epsilon_F = 2.5$ and $\delta_0/\epsilon_F = 0.5$, respectively, with a relative difference of $0.75/0.92 \sim 0.81$.

Therefore, even though the Hopfield coefficients somewhat depend on δ_0, the values of Δ_M in the optimal pairing regime of $E_{\text{gap}}/\epsilon_F \sim 0.25$ depend solely on E_{gap}. This implies that it is the reduced retardation effects, arising from finite E_{gap}, that dictate the pairing physics and the effect of $\mathcal{C}_0^2$ is relatively small. Only at larger E_{gap} the values of Δ_M in case of different δ_0 start to gradually deviate from each other [see Fig. 2(a) of the main text]. From Fig. 2(a) of the main text, we see that Δ_M at the large-E_{gap} regime is highest for larger δ_0, consistent with the values of $\mathcal{C}_0^2$ shown in Fig. 6. The behavior of $\mathcal{C}_0^2$ therefore matters only at the large E_{gap} regime. As we are interested in the optimal pairing regime of $E_{\text{gap}}/\epsilon_F \sim 0.25$, the effect of $\mathcal{C}_0^2$ can then be safely ignored when discussing the qualitative properties of the pairing interaction.

3. Effective interaction range

As we mentioned in the main text, one can approximate the polariton dispersion as $\epsilon_k^{LP} \approx \epsilon_k^x - E_{\text{gap}}\delta_{k,0}$. We have numerically furthermore confirmed that excluding the zero momentum does not play a role in the Eliashberg calculation so we can safely take $\tilde{\epsilon}_k^{LP} \approx \epsilon_k^x + E_{\text{gap}}$. With this expression, one obtains the range ξ of the static interaction $V_{\text{ind}}(\mathbf{k}, 0)$ as $(C_k \approx 1)$

$$\xi \sim \frac{1}{\sqrt{E_{\text{gap}}\left(\frac{2}{\mathcal{C}_0^2} - 1\right) + 2g_{xx}\mathcal{C}_0^2 n_0}}. \quad (A9)$$

With $\mathcal{C}_0^2 \sim 1$, this is the same result as mentioned in the main text. We see from Eq. (A9) that both E_{gap} and n_0 tend to suppress the interaction range. This can be qualitatively understood by the fact that both the quantities increase the energies of the Bogoliubov excitation modes at momenta relevant for the pairing. Thus, the exchange of the sound modes is suppressed and the range therefore decreased.

APPENDIX B: ELIASHBERG EQUATIONS

Eliashberg equations shown in the main text can be derived by writing down the perturbation series for the normal and anomalous Green's functions of the electrons as [67]

$$G_{11}(\mathbf{k}, \tau) = \frac{1}{\langle e^{-\beta H}\rangle_0} \sum_{n=0} \frac{(-1)^n}{n!} \int_0^\beta d\tau_1 \cdots \int_0^\beta d\tau_n$$
$$\times \langle -T_\tau H_{\text{int}}(\tau_1)\cdots H_{\text{int}}(\tau_n)\hat{e}_\mathbf{k}(\tau)\hat{e}_\mathbf{k}^\dagger\rangle_0, \quad (B1)$$

$$G_{12}(\mathbf{k}, \tau) = \frac{1}{\langle e^{-\beta H}\rangle_0} \sum_{n=0} \frac{(-1)^n}{n!} \int_0^\beta d\tau_1 \cdots \int_0^\beta d\tau_n$$
$$\times \langle -T_\tau H_{\text{int}}(\tau_1)\cdots H_{\text{int}}(\tau_n)\hat{e}_\mathbf{k}(\tau)\hat{e}_{-\mathbf{k}}\rangle_0, \quad (B2)$$

and keeping the terms involving the Fock diagrams [48]. Here $\langle \cdots \rangle_0$ denotes the average with respect to the noninteracting Hamiltonian, and furthermore we have defined $H_{\text{int}}(\tau) = \int_0^\beta d\tau' \frac{1}{2} \sum_{\mathbf{k},\mathbf{k}',\mathbf{q}} V_{\text{tot}}(\mathbf{q}, \tau - \tau')\hat{e}_{\mathbf{k}+\mathbf{q}}^\dagger(\tau')\hat{e}_{\mathbf{k}'-\mathbf{q}}^\dagger(\tau)\hat{e}_{\mathbf{k}'}(\tau)\hat{e}_\mathbf{k}(\tau')$ and $V_{\text{tot}}(\mathbf{q}, \tau) = V_{\text{ind}}(\mathbf{q}, \tau) + V_C(\mathbf{q})\delta(\tau - \tau')$ with $V_C(\mathbf{q})$ being the screened Coulomb interaction, i.e., the second term in Eq. (3) of the main text.
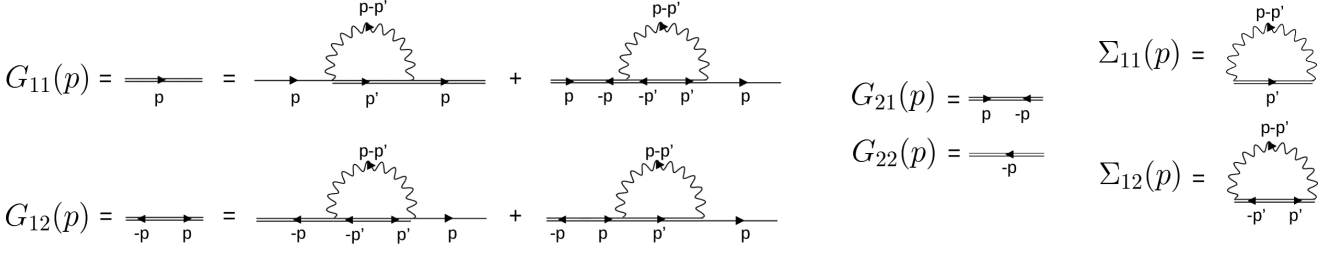
FIG. 7. Feynman diagrams for $G_{11}(p)$ and $G_{12}(p)$ as well as for the self-energies $\Sigma_{11}(p)$ and $\Sigma_{12}(p)$. Single lines, double lines, and wavy lines represent noninteracting propagators $G_{11}^0(p)$, interacting propagators $G_{ij}(p)$, and effective electron-electron interactions $V_{\text{tot}}(p)$, respectively.

As a result, one finds the diagrammatic presentation shown in Fig. 7. Explicitly, the Green's functions in the Matsubara space then read

$$G_{11}(p) = G_{11}^0(p) + G_{11}^0(p)\Sigma_{11}(p)G_{11}(p) + G_{11}^0(p)\Sigma_{12}(p)G_{21}(p), \tag{B3}$$

$$G_{12}(p) = G_{11}^0(p)\Sigma_{12}(p)G_{22}(p) + G_{11}^0(p)\Sigma_{11}(p)G_{12}(p), \tag{B4}$$

where we have used the short-hand notation $p \equiv (\mathbf{p}, ip_n)$ with p_n being a fermionic Matsubara frequency. The self-energies $\Sigma_{ij}(k)$ are defined as in the main text and the noninteracting Green's function reads $G_{11}^0(p) = 1/(ip_n - \epsilon_{\mathbf{p}}^e + \mu_e)$. By using the identities $G_{21}(p) = G_{12}^*(p)$, $G_{ii}^*(p) = G_{ii}(-p)$, $G_{22}(p) = -G_{11}^*(p)$ and the fact that $V_{\text{ind}}(p) = V_{\text{ind}}(-p)$, we can write the Dyson equation as

$$G(p) = \begin{bmatrix} G_{11}(p) & G_{12}(p) \\ G_{12}(p) & G_{22}(p) \end{bmatrix} = G^0(p) + G^0(p)\Sigma(p)G(p), \tag{B5}$$

where $[G^0(p)]_{ij} = G_{ii}^0(p)\delta_{ij}$. By solving $G(p)$ from Eq. (B5), one obtains the equations given in the main text.

APPENDIX C: MOMENTUM DEPENDENCE OF THE GAP AND FERMI SURFACE DEFORMATION

The superconducting critical temperature T_c we obtain from our Eliashberg theory is unusually small compared to the maximum of the order parameter Δ_M. The ratio of these quantities is $k_B T_c / \Delta_M \sim 0.044$, which is an order of magnitude lower than the BCS result 0.57 [48]. However, in the usual BCS theory, the gap is assumed to be constant in the momentum and frequency spaces. Momentum-independent order parameter implies spatially small and tightly bounded Cooper pairs. In our case, the pairing gap depends strongly on the momentum as can be seen from Fig. 8(a), where we have plotted the maximum of the pairing gap as a function of the momentum in case of three different values of E_{gap}. The gap is far from being constant and is strongly peaked near the Fermi surface. Cooper pairs are therefore more loosely bound than in case of the constant BCS gap.

The BCS theory also ignores the frequency dependency of the pairing interaction. Frequency dependent interaction in turn leads to the retardation effects and finite diagonal self-energy $\Sigma_{11}(p)$. To demonstrate this in a simple way, we note that $\Sigma_{11}(p) = -\Sigma_{11}(-p)$, where we have used the

properties $G_{11}(p) = -G_{11}(-p)$ and $V_{\text{tot}}(p) = V_{\text{tot}}(-p)$. Furthermore, as evidently $\Sigma_{11}(\mathbf{p}, p_n) = \Sigma_{11}(-\mathbf{p}, p_n)$, it is clear that $\Sigma_{11}(p) = 0$ if the interaction V_{tot} is frequency independent. Retarded interaction of Eq. (A8) therefore gives a rise for finite $\Sigma_{11}(p)$. Moreover, it is easy to see that retardation also causes the frequency dependence of the pairing gap $\Delta(p)$.

The frequency dependence of the diagonal self-energy leads to the deformation of the Fermi surface, which in turn suppresses the formation of Cooper pairs, as the sharp Fermi surface is key to the pairing instability [48]. This manifests in Fig. 3(c) of the main text where we see how seriously deformed the Fermi surface is; the occupation number $n_{\mathbf{k}}$ for small $\mathbf{k}$ does not reach even the half-filling even though the temperature is very low ($\epsilon_F / T = 50$). By increasing E_{gap}, we can make the interaction V_{ind} less frequency-dependent [as demonstrated in Figs. 3(a) and 3(b) of the main text] and in that way make the reduce the diagonal self-energy. This is shown in Fig. 8(b) where the real and imaginary parts of $\Sigma_{11}(\mathbf{k}, k_1)$ is depicted for three E_{gap} [same δ_0 and Ω as in Fig. 3(c) of the main text and Fig. 8(a)]. We see that increasing E_{gap} reduces Σ_{11} and thus makes the Fermi surface sharper as shown in Fig. 3(c) of the main text.
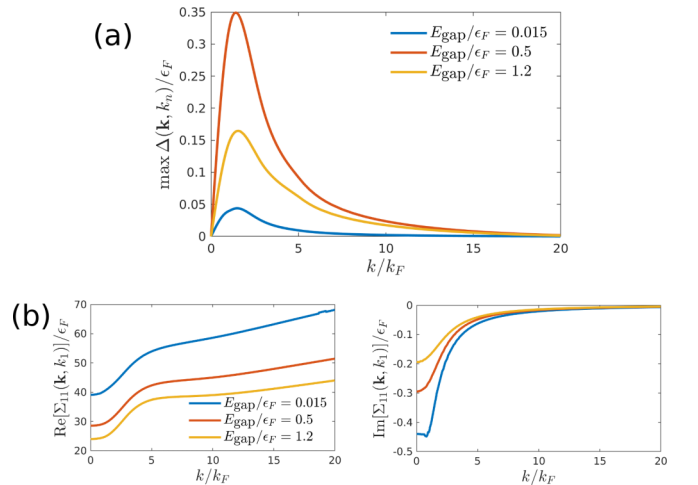

FIG. 8. (a) The maximum of the pairing gap as a function of momentum $\mathbf{k}$ for a few values of E_{gap} corresponding to $\delta_0 / \epsilon_F = 1$ and $\Omega / \epsilon_F = 0.125, 0.875,$ and 1.625. (b) Corresponding real (left panel) and imaginary (right panel) parts of the diagonal self-energy $\Sigma_{11}(\mathbf{k}, k_1)$.

[1] G. Wang, A. Chernikov, M. M. Glazov, T. F. Heinz, X. Marie, T. Amand, and B. Urbaszek, Rev. Mod. Phys. **90**, 021001 (2018).

[2] T. Mueller and E. Malic, npj 2D Mater. Appl. **2**, 29 (2018).

[3] C. Schneider, M. M. Glazov, T. Korn, S. Höfling, and B. Urbaszek, Nat. Commun. **9**, 2695 (2018).

[4] D. Xiao, G.-B. Liu, W. Feng, X. Xu, and W. Yao, Phys. Rev. Lett. **108**, 196802 (2012).

[5] T. Cao, G. Wang, W. Han, H. Ye, C. Zhu, J. Shi, Q. Niu, P. Tan, E. Wang, B. Liu, and J. Feng, Nat. Commun. **3**, 887 (2012).

[6] H. Zeng, J. Dai, W. Yao, D. Xiao, and X. Cui, Nat. Nanotechnol. **7**, 490 (2012).

[7] K. F. Mak, K. He, J. Shan, and T. F. Heinz, Nat. Nanotechnol. **7**, 494 (2012).

[8] J. R. Schaibley, H. Yu, G. Clark, P. Rivera, J. S. Ross, K. L. Seyler, W. Yao, and X. Xu, Nat. Rev. Mater. **1**, 16055 (2016).

[9] S. Dufferwiel, S. Schwarz, F. Withers, A. A. P. Trichet, F. Li, M. Sich, O. Del Pozo-Zamudio, C. Clark, A. Nalitov, D. D. Solnyshkov *et al.*, Nat. Commun. **6**, 8579 (2015).

[10] A. V. Kavokin, J. J. Baumberg, G. Malpuech, and F. P. Laussy, *Microcavities*, Series on Semiconductor Science and Technology (Oxford University Press, Oxford, 2017)

[11] M. Sidler, P. Back, O. Cotlet, A. Srivastava, T. Fink, M. Kroner, E. Demler, and A. Imamoglu, Nat. Phys. **13**, 255 (2017).

[12] L. B. Tan, O. Cotlet, A. Bergschneider, R. Schmidt, P. Back, Y. Shimazaki, M. Kroner, and A. Imamoglu, Phys. Rev. X **10**, 021011 (2020).

[13] R. P. A. Emmanuele, M. Sich, O. Kyriienko, V. Shahnazaryan, F. Withers, A. Catanzaro, P. M. Walker, F. A. Benimetskiy, M. S. Skolnick, A. I. Tartakovskii *et al.*, Nat. Commun. **11**, 3589 (2020).

[14] C. Anton-Solanas, M. Waldherr, M. Klaas, H. Suchomel, T. H. Harder, H. Cai, E. Sedov, S. Klembt, A. V. Kavokin, S. Tongay *et al.*, Nat. Mater. **20**, 1233 (2021).

[15] M. A. Bastarrachea-Magnani, A. Camacho-Guardian, M. Wouters, and G. M. Bruun, Phys. Rev. B **100**, 195301 (2019).

[16] M. A. Bastarrachea-Magnani, A. Camacho-Guardian, and G. M. Bruun, Phys. Rev. Lett. **126**, 127405 (2021).

[17] A. Julku, M. A. Bastarrachea-Magnani, A. Camacho-Guardian, and G. M. Bruun, Phys. Rev. B **104**, L161301 (2021).

[18] J. W. Park, C.-H. Wu, I. Santiago, T. G. Tiecke, S. Will, P. Ahmadi, and M. W. Zwierlein, Phys. Rev. A **85**, 051602(R) (2012).

[19] M.-S. Heo, T. T. Wang, C. A. Christensen, T. M. Rvachov, D. A. Cotta, J.-H. Choi, Y.-R. Lee, and W. Ketterle, Phys. Rev. A **86**, 021602(R) (2012).

[20] I. Ferrier-Barbut, M. Delehaye, S. Laurent, A. T. Grier, M. Pierce, B. S. Rem, F. Chevy, and C. Salomon, Science **345**, 1035 (2014).

[21] V. D. Vaidya, J. Tiamsuphat, S. L. Rolston, and J. V. Porto, Phys. Rev. A **92**, 043604 (2015).

[22] B. J. DeSalvo, K. Patel, J. Johansen, and C. Chin, Phys. Rev. Lett. **119**, 233401 (2017).

[23] R. S. Lous, I. Fritsche, M. Jag, F. Lehmann, E. Kirilov, B. Huang, and R. Grimm, Phys. Rev. Lett. **120**, 243403 (2018).

[24] F. Schäfer, N. Mizukami, P. Yu, S. Koibuchi, A. Bouscal, and Y. Takahashi, Phys. Rev. A **98**, 051602(R) (2018).

[25] D. K. Efimkin and A. H. MacDonald, Phys. Rev. B **95**, 035417 (2017).

[26] V. Shahnazaryan, V. K. Kozin, I. A. Shelykh, I. V. Iorsh, and O. Kyriienko, Phys. Rev. B **102**, 115310 (2020).

[27] J. von Milczewski, F. Rose, and R. Schmidt, Phys. Rev. A **105**, 013317 (2022).

[28] I. A. Shelykh, T. Taylor, and A. V. Kavokin, Phys. Rev. Lett. **105**, 140402 (2010).

[29] M. Matuszewski, T. Taylor, and A. V. Kavokin, Phys. Rev. Lett. **108**, 060401 (2012).

[30] V. Kovalev and A. Chaplik, JETP Lett. **94**, 560 (2011).

[31] K. H. A. Villegas, M. Sun, V. M. Kovalev, and I. G. Savenko, Phys. Rev. Lett. **123**, 095301 (2019).

[32] M. V. Boev, V. M. Kovalev, and I. G. Savenko, Phys. Rev. B **99**, 155409 (2019).

[33] F. P. Laussy, A. V. Kavokin, and I. A. Shelykh, Phys. Rev. Lett. **104**, 106402 (2010).

[34] O. Cotleţ, S. Zeytinoğlu, M. Sigrist, E. Demler, and A. Imamoğlu, Phys. Rev. B **93**, 054510 (2016).

[35] H. Zhang, C.-X. Liu, S. Gazibegovic, D. Xu, J. A. Logan, G. Wang, N. van Loo, J. D. S. Bommer, M. W. A. de Moor, D. Car *et al.*, Nature (London) **556**, 74 (2018). **591**, E30 (2021).

[36] S. Vaitiekėnas, G. W. Winkler, B. van Heck, T. Karzig, M.-T. Deng, K. Flensberg, L. I. Glazman, C. Nayak, P. Krogstrup, R. M. Lutchyn, and C. M. Marcus, Science **367**, eaav3392 (2020); H. H. Thorp, *ibid.* **373**, 500 (2021).

[37] Q. L. He, L. Pan, A. L. Stern, E. C. Burks, X. Che, G. Yin, J. Wang, B. Lian, Q. Zhou, E. S. Choi *et al.*, Science **357**, 294 (2017). H. H. Thorp, *ibid.* **374**, 1454 (2021).

[38] A. Chronister, A. Pustogow, N. Kikugawa, D. A. Sokolov, F. Jerzembeck, C. W. Hicks, A. P. Mackenzie, E. D. Bauer, and S. E. Brown, Proc. Natl. Acad. Sci. USA **118**, e2025313118 (2021).

[39] A. Chernikov, T. C. Berkelbach, H. M. Hill, A. Rigosi, Y. Li, O. B. Aslan, D. R. Reichman, M. S. Hybertsen, and T. F. Heinz, Phys. Rev. Lett. **113**, 076802 (2014).

[40] D. K. Efimkin, E. K. Laird, J. Levinsen, M. M. Parish, and A. H. MacDonald, Phys. Rev. B **103**, 075417 (2021).

[41] A. Kormányos, G. Burkard, M. Gmitra, J. Fabian, V. Zólyomi, N. D. Drummond, and V. Fal'ko, 2D Mater. **2**, 022001 (2015).

[42] F. Barachati, A. Fieramosca, S. Hafezian, J. Gu, B. Chakraborty, D. Ballarini, L. Martinu, V. Menon, D. Sanvitto, and S. Kéna-Cohen, Nat. Nanotechnol. **13**, 906 (2018).

[43] J. J. Hopfield, Phys. Rev. **112**, 1555 (1958).

[44] A. Camacho-Guardian, M. A. Bastarrachea-Magnani, and G. M. Bruun, Phys. Rev. Lett. **126**, 017401 (2021).

[45] Z. Wu and G. M. Bruun, Phys. Rev. Lett. **117**, 245302 (2016).

[46] A. Strashko, F. M. Marchetti, A. H. MacDonald, and J. Keeling, Phys. Rev. Lett. **125**, 067405 (2020).

[47] O. Cotlet, D. S. Wild, M. D. Lukin, and A. Imamoglu, Phys. Rev. B **101**, 205409 (2020).

[48] G. D. Mahan, *Many-Particle Physics* (Plenum, New York, 2000).

[49] J. J. Kinnunen, Z. Wu, and G. M. Bruun, Phys. Rev. Lett. **121**, 253402 (2018).

[50] T. Chervy, P. Knüppel, H. Abbaspour, M. Lupatini, S. Fält, W. Wegscheider, M. Kroner, and A. Imamoğlu, Phys. Rev. X **10**, 011040 (2020).

[51] I. Carusotto and C. Ciuti, Rev. Mod. Phys. **85**, 299 (2013).

[52] I. Schwartz, Y. Shimazaki, C. Kuhlenkamp, K. Watanabe, T. Taniguchi, M. Kroner, and A. Imamoğlu, Science **374**, 336 (2021).

[53] C. Kuhlenkamp, M. Knap, M. Wagner, R. Schmidt, and A. Imamoğlu, Phys. Rev. Lett. **129**, 037401 (2022).

[54] Y. Tang, L. Li, T. Li, Y. Xu, S. Liu, K. Barmak, K. Watanabe, T. Taniguchi, A. H. MacDonald, J. Shan, and K. F. Mak, Nature (London) **579**, 353 (2020).

[55] E. C. Regan, D. Wang, C. Jin, M. I. Bakti Utama, B. Gao, X. Wei, S. Zhao, W. Zhao, Z. Zhang, K. Yumigeta *et al.*, Nature (London) **579**, 359 (2020).

[56] L. Wang, E.-M. Shih, A. Ghiotto, L. Xian, D. A. Rhodes, C. Tan, M. Claassen, D. M. Kennes, Y. Bai, B. Kim *et al.*, Nat. Mater. **19**, 861 (2020).

[57] K. Tran, G. Moody, F. Wu, X. Lu, J. Choi, K. Kim, A. Rai, D. A. Sanchez, J. Quan, A. Singh *et al.*, Nature (London) **567**, 71 (2019).

[58] E. M. Alexeev, D. A. Ruiz-Tijerina, M. Danovich, M. J. Hamer, D. J. Terry, P. K. Nayak, S. Ahn, S. Pak, J. Lee, J. I. Sohn *et al.*, Nature (London) **567**, 81 (2019).

[59] Y. Shimazaki, I. Schwartz, K. Watanabe, T. Taniguchi, M. Kroner, and A. Imamoğlu, Nature (London) **580**, 472 (2020).

[60] K. L. Seyler, P. Rivera, H. Yu, N. P. Wilson, E. L. Ray, D. G. Mandrus, J. Yan, W. Yao, and X. Xu, Nature (London) **567**, 66 (2019).

[61] C. Jin, E. C. Regan, A. Yan, M. Iqbal Bakti Utama, D. Wang, S. Zhao, Y. Qin, S. Yang, Z. Zheng, S. Shi *et al.*, Nature (London) **567**, 76 (2019).

[62] T. T. Heikkilä, N. B. Kopnin, and G. E. Volovik, JETP Lett. **94**, 233 (2011).

[63] N. B. Kopnin, T. T. Heikkilä, and G. E. Volovik, Phys. Rev. B **83**, 220503 (2011).

[64] S. Peotta and P. Törmä, Nat. Commun. **6**, 8944 (2015).

[65] L. Liang, T. I. Vanhala, S. Peotta, T. Siro, A. Harju, and P. Törmä, Phys. Rev. B **95**, 024515 (2017).

[66] X. Wang, C. Xiao, H. Park, J. Zhu, C. Wang, T. Taniguchi, K. Watanabe, J. Yan, D. Xiao, D. R. Gamelin *et al.*, Nature (London) **604**, 468 (2022).

[67] H. Bruus and K. Flensberg, *Many-Body Quantum Theory in Condensed Matter Physics* (Oxford University Press, Oxford, 2004).

[68] A. Fetter and J. Walecka, *Quantum Theory of Many-Particle Systems*, Dover Books on Physics Series (Dover Publications, New York, 1971).